PHYSICAL REVIEW B VOLUME 27, NUMBER 2 15 JANUARY 1983

Scattering by ionization and phonon emission in semiconductors. II. Monte Carlo calculations

R. Casanova Alig
RCA Laboratories, Princeton, New Jersey 08540
(Received 30 August 1982)

Calculations of the pair-creation energy ϵ and the Fano factor F for semiconductors are done for the assumptions that in each scattering event all possible sets of product particles are equally probable, that the energy bands are those of free particles separated by a band gap E_g, and that there is a single phonon energy $\hbar\omega_0$. The results from calculations done previously with the use of a recursive method are corroborated and expanded with the use of the Monte Carlo method. The electron-phonon interaction is divided into a deformation-potential interaction and a polar-mode electrostatic interaction, and the $\hbar\omega_0$ dependence of these interactions is incorporated into the calculations. New values of ϵ and F are calculated. For many semiconductors, the accord of these values with experiments is as good as the accord of previous calculations done with the deformation potential alone, indicating the insensitivity of ϵ to the added interaction.

I. INTRODUCTION

Calculations of the pair-creation energy ϵ and the Fano factor F in semiconductors are described in a previously published paper.[1] These quantities are measured when high-energy electrons and holes scatter by ionization and by phonon emission. The calculations were done using a recursive method to calculate the scattering probabilities. Although the recursive method was well suited to demonstrate the conclusions of that study, i.e., the insensitivity of ϵ and F to electron energy loss to plasmons and to differences in the threshold energy for ionization, it is cumbersome both to describe and to use. An alternative method, the Monte Carlo method, to calculate ϵ and F is used here. It is obvious in description and simple to apply. It yields the same values of ϵ and F as the recursive method, confirming the earlier calculations. In addition, quantities that were difficult to obtain with the recursive method are easily obtained with the Monte Carlo method.

After the Monte Carlo method has been introduced, it will be applied to the calculation of scattering rates due to both the deformation-potential electron-phonon interaction, described in the earlier report,[1] and to the polar-mode electrostatic electron-phonon interaction, which is introduced here. New lower limits on ϵ are calculated. Although they are generally larger than those reported earlier because of the additional interaction, they are not much larger. Hence ϵ is not sensitive to this additional scattering. In particular, the upper bounds on the cathodoluminescent efficiency, which varies inversely with ϵ, still exceed the maximum measured efficiencies.

The Monte Carlo method is described in Sec. II. The Monte Carlo method was also used by van Roosbroeck[2] to verify the analysis he called "crazy carpentry." The scattering rate assumption used here and in Ref. 1 is equivalent to the assumption used by van Roosbroeck.[3] Thus when the different assumptions used to do the calculations here and in Ref. 2 are taken into account, direct comparisons of the calculations are possible. These comparisons are discussed in Sec. IV of this paper.

In Sec. III the polar-mode electrostatic electron-phonon interaction is introduced. The matrix elements for both the deformation-potential and the polar-mode electrostatic electron-phonon interactions, as evaluated in the free-particle approximation, are described. The matrix element for the deformation-potential interaction is introduced in the same manner as in Ref. 1. The matrix element for the polar-mode electrostatic interaction is then introduced in an analogous manner.

In Ref. 1 an empirical constant, labeled A, was introduced to describe the ratio of the matrix elements for the electron-phonon interaction and the Coulomb interaction. Here, this constant A is restricted to the deformation-potential part of the electron-phonon interaction, and a second empirical constant, labeled B, is introduced. By analogy, it is the ratio of the matrix elements of the polar-mode electrostatic interaction and the Coulomb interaction.

The matrix elements of the deformation-potential and polar-mode electrostatic interactions, considered now in the free-particle approximation, have dif-

 ©1983 The American Physical Society

ferent dependences on the phonon energy $\hbar\omega_0$, and so the ratios of these two scattering rates to the ionization scattering rate have different dependences on $\hbar\omega_0$. Therefore the phonon energy has been removed from the constants A and B, and new constants A' and B' are defined. This modification is necessary to have a consistent theory with $\hbar\omega_0$ as a parameter.

Following the procedure of Ref. 1, the constant A' is assumed to be independent of the particle energy and invariant for electrons and holes, for different materials, and for all ambient conditions. A similar assumption is made about B'. Following Ref. 1 the constant A' is fixed from the measured value of ϵ for Si. In Si, of course, the polar-mode electrostatic interaction is zero. Then, using the above assumption, A' is given the same value in CdS as in Si. The additional phonon scattering required to calculate a value of ϵ for CdS equal to the measured value is then used to fix the constant B'. These values of A' and B' are used in the subsequent calculations for other semiconductors. The new calculations of ϵ and those of Ref. 1 agree with the measured values equally well.

II. MONTE CARLO METHOD

A. Method

The Monte Carlo method consists of simulating random microscopic processes a large number of times. Macroscopic properties may then be determined by averaging over the large number of simulations. Each simulation consists of a cascade such as that shown in Fig. 1 of Ref. 1. An incident particle, or primary, enters the semiconductor with an energy E that is large compared to the semiconductor band gap. It scatters by ionization, i.e., by creating electron-hole pairs, and by phonon emission to generate a number of thermalized electron-hole pairs. The probability that n such pairs are created was denoted $p_n(E)$ and was called the pair-number probability distribution in Ref. 1. In the Monte Carlo method, the fraction of the simulations yielding n pairs is $p_n(E)$.

The calculation of ϵ and F was done with the definitions

$$\epsilon = \frac{E}{\langle n(E)\rangle} \tag{1}$$

and

$$F = \frac{\langle n^2(E)\rangle - \langle n(E)\rangle^2}{\langle n(E)\rangle} , \tag{2}$$

where

$$\langle n(E)\rangle = \sum_{n=0}^{\infty} n p_n(E) \tag{3}$$

and

$$\langle n^2(E)\rangle = \sum_{n=0}^{\infty} n^2 p_n(E) \tag{4}$$

are the first and second moments of $p_n(E)$, respectively.

The scattering-rate assumption from Ref. 1 was used to generate each cascade. Under this assumption, in each ionization scattering event of a cascade, all the states available to the three product particles have equal probabilities to be filled. The selection of the three states which are filled from the many available states is the random feature of this calculation. Since the available states are not distributed uniformly in energy, but the random numbers are uniformly distributed on the unit interval, an association between a randomly generated number and the energy of a state must be developed. This association is described in the next section.

B. Ionization scattering

When a particle of energy E scatters by ionization, three particles (the particle plus the electron and hole created by ionization) are created, with kinetic energies E_1, E_2, and $E-E_1-E_2-E_g$, where E_g is the semiconductor band gap. With the use of the scattering-rate assumption, the probability dq_1 that a particle of energy E scatters to create a particle with energy between E_1 and E_1+dE_1 is

$$dq_1 = \frac{\rho(E_1)f(E_1)dE_1}{\int dE_1 \rho(E_1)f(E_1)} , \tag{5}$$

where

$$f(E_1) = \int dE_2 \int dE_3 \rho(E_2)\rho(E_3) \times \delta(E-E_g-E_1-E_2-E_3)$$

and $\rho(E)$ is the density of states. In the free-particle model in which the band structures of the conduction and valence bands are isotropic and parabolic, $\rho(E)$ is proportional to $\sqrt{E}$. Then, following Eq. (18) of Ref. 1,

$$\begin{aligned} dq_1 &= \frac{105}{2\pi}(E-E_g)^{-7/2}\sqrt{E_1}\,dE_1 \\ &\quad \times \int_0^{E-E_g-E_1} \sqrt{E_2}(E-E_g-E_1-E_2)^{1/2} dE_2 \\ &= \tfrac{105}{16}(1-\alpha_1)^2\sqrt{\alpha_1}\,d\alpha_1 , \end{aligned} \tag{6}$$

where $\alpha_1 = E_1/(E-E_g)$, so $0 \le \alpha_1 \le 1$. Since all available states are equally probable, they will be occupied randomly, and the energy E_1 of the state as-

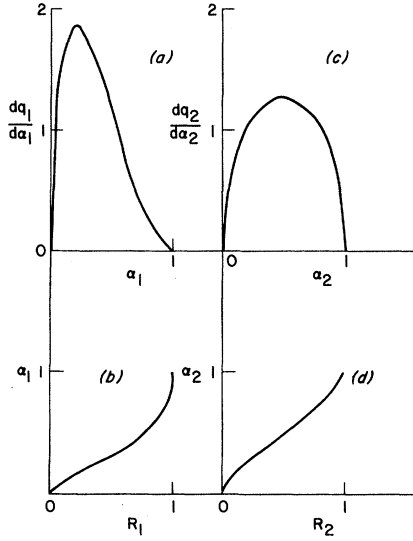

FIG. 1. (a) Plot of $dq_1/d\alpha_1$ vs α_1 as given by Eq. (6). (b) Plot of $\alpha_1(R_1)$, the inverse of the function shown in Eq. (7). All values of R_1 occur with equal probability; thus large values of $E_1=\alpha_1(E-E_g)$ are less likely than small values. (c) Plot of $dq_2/d\alpha_2$ vs α_2 as given by Eq. (9). (d) Plot of $\alpha_2(R_2)$, the inverse of the function shown in Eq. (10).

sociated with the random number R_1 is given by $\alpha_1(R_1)$ where

$$R_1=\int_0^{R_1} dq_1=\int_0^{\alpha_1}\left[\frac{dq_1}{d\alpha_1}\right]d\alpha_1$$

$$=\tfrac{105}{8}\alpha_1^{3/2}\left[\frac{\alpha_1^2}{7}-\frac{2\alpha_1}{5}+\frac{1}{3}\right]. \quad (7)$$

This equation was inverted numerically to obtain $\alpha_1(R_1)$, which is used to associate the randomly generated number R_1 with the energy E_1 assigned to one of the scattered particles. The functions $dq_1/d\alpha_1$ and $\alpha_1(R_1)$ are shown in Fig. 1. The peak in $dq_1/d\alpha_1$ at low energies, for which there are relatively few states, arises because three particles leave each scattering event, and if one has a low energy, the remaining two have a larger energy that can be divided between more pairs of states.

Again using the scattering-rate assumption, the probability dq_2 that a particle of energy E creates a particle of energy E_1 while it scatters to a state of energy between E_2 and E_2+dE_2 is

$$dq_2=\frac{\rho(E_2)g(E_1,E_2)dE_2}{\int dE_2\rho(E_2)g(E_1,E_2)}, \quad (8)$$

where

$$g(E_1,E_2)=\int dE_3\rho(E_3)\delta(E-E_g-E_1-E_2-E_3)$$
$$=\rho(E-E_g-E_1-E_2).$$

In the free-particle model,

$$dq_2=\frac{\sqrt{E_2}(E-E_g-E_1-E_2)^{1/2}dE_2}{(\pi/8)(E-E_g-E_1)^2}$$
$$=(8/\pi)\sqrt{\alpha_2}(1-\alpha_2)^{1/2}d\alpha_2, \quad (9)$$

where $\alpha_2=E_2/(E-E_g-E_1)$ so $0\le\alpha_2\le1$. Again, since all available states are equally probable, they will be occupied randomly, and the energy E_2 of the state associated with the random number R_2 is given by $\alpha_2(R_2)$, where

$$R_2=\int_0^{R_2} dq_2=\int_0^{\alpha_2}\left[\frac{dq_2}{d\alpha_2}\right]d\alpha_2$$
$$=(2/\pi)(2\alpha_2-1)\sqrt{\alpha_2}(1-\alpha_2)^{1/2}$$
$$+\pi^{-1}\sin^{-1}(2\alpha_2-1)+\tfrac{1}{2}. \quad (10)$$

This equation was inverted numerically to obtain $\alpha_2(R_2)$, which is used to associate the randomly generated number R_2 with energy E_2 to be assigned to another of the scattered particles. The functions $dq_2/d\alpha_2$ and $\alpha_2(R_2)$ are shown in Fig. 1. The function $dq_2/d\alpha_2$ is symmetric about $\alpha_2=0.5$, as expected when two particles occupy pairs of states with constant total energy.

C. Comparison with the recursive method

A particle of energy E may also scatter by the emission of a phonon with energy $\hbar\omega_0$. The rates of scattering by phonon emission and by ionization were related in Ref. 1 by an empirical constant A, defined by Eqs. (20) and (21) of Ref. 1. Randomly generated numbers were used with Eq. (20) of Ref. 1 to assign each scattering event to ionization or phonon emission. If a given scattering event resulted in ionization, the procedure described in the preceding section was used to find the energies of the scattered particles. If it resulted in a phonon emission, the scattered particle was assigned the energy $E-\hbar\omega_0$.

The random numbers were generated with a library subroutine.[4] Calculations were done to verify that the Monte Carlo method gives the same values for ϵ and F as the recursive method used in Ref. 1. The threshold energies from Eq. (23) of Ref. 1, those obtained by neglecting momentum conservation,

were used in all these calculations and the plasmon energy was ignored. Thus in the notation of Ref. 1, the overscored and unsubscripted values of ϵ and F were calculated; the overscore will not be used in this paper.

In the Monte Carlo method only the mean values of ϵ and F can be calculated. There will be uncertainties in the values related to the initial energy E of each cascade and the number N of cascades calculated. These uncertainties were taken at the 95% confidence level. The number of cascades was limited by the cost of computer time. No calculation was allowed to run much in excess of 100 CPU sec on an IBM 370. As a result N never exceeded 10 000, and it has to be restricted to smaller values when E exceeded $50E_g$. The initial energy of each cascade is limited by the capacity of the computer memory to retain the energies of all the particles in the cascade. This limit is about 100 000 pairs per cascade.

The values calculated for $\epsilon(E)$ and $F(E)$ for $E \leq 12E_g$ using the Monte Carlo method agree, within the 95% confidence level, with the values given in Ref. 1. Calculations were done for Si using $A=5.2$ eV^3 and $A=0$, and the uncertainties in $\epsilon(E)$ were less than 1% of the mean values for $E \geq 4$ eV; the uncertainties in $F(E)$ were less than 6%. The values calculated for $p_n(E)$ also agree with those calculated in Ref. 1.

As was pointed out in Ref. 1, calculations for E much larger than $10E_g$ are prohibitively expensive with the recursive method. With the Monte Carlo method, however, only the computer memory limits the initial energies for which $\epsilon(E)$ can be calculated, and calculations for E up to and beyond $100\,000E_g$ are easily done. Thus calculations which are difficult with the recursive method are easy with the Monte Carlo method. There are, of course, other calculations which are difficult with the Monte Carlo method, but easy with the recursive method, as, for example, calculations of $\epsilon_{\bar{k}}(E)$ as given in Eq. (25) of Ref. 1, which requires integration of $p_n(E)$ over E.

Since the uncertainty in $\epsilon(E)$ depends only on the number of pairs calculated, values of $\epsilon(E)$ with uncertainies below 1% of the mean can be calculated for large values of E. The plot of $\epsilon(E)$ shown in Figs. 2 and 5 of Ref. 1 is extended up to 10 000 eV in Fig. 2. However, the uncertainity in $F(E)$ depends on the number of cascades, and for reasons of cost, the number of cascades had to be severely restricted for values of E above $200E_g$. Thus values of $F(E)$ with uncertainties below 10% of the mean can only be calculated for $E \leq 200E_g$. Likewise, since the accuracy of the values of $p_n(E)$ for a given E depend on the number of cascades, accurate values can only be calculated for $E \leq 200E_g$. The calculated

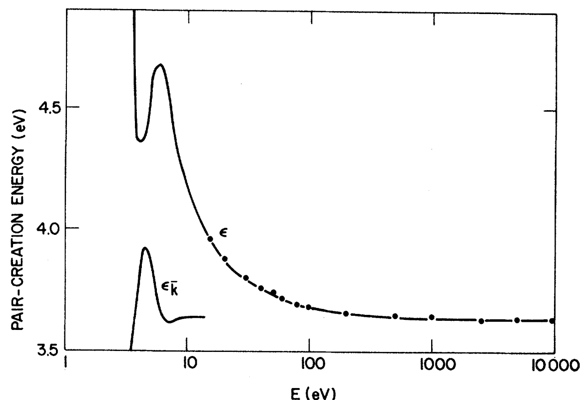

FIG. 2. Pair-creation energy $\epsilon(E)$ is plotted vs E. The values were calculated for $A=5.2$ eV^3 for the band gap and phonon energy of Si. The points show the Monte Carlo calculations. The values for $E \leq 15$ eV differ little from the values shown in Figs. 2 and 5 of Ref. 1. The asymptotic behavior for large E was verified by a calculation for 0.3 MeV. The function $\epsilon_{\bar{k}}(E)$ from Fig. 5 of Ref. 1 is repeated here.

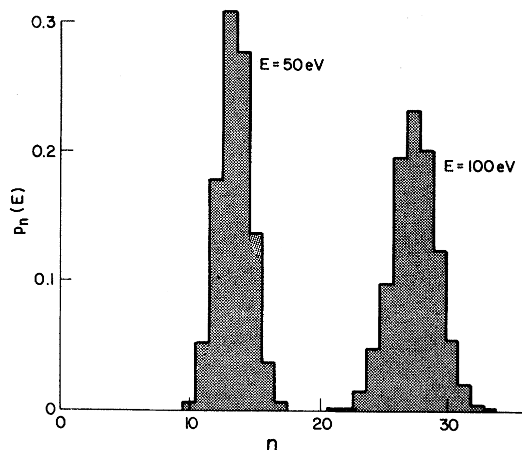

FIG. 3. Calculated values of the pair-number probability distributions p_n (50 eV) and p_n (100 eV) for Si as calculated with the Monte Carlo method. The values of $\langle n \rangle$ and $\langle n^2 \rangle$ in Eqs. (3) and (4) are the first and second moments of these histograms. For a primary energy of 50 eV, $\langle n \rangle = 13.38$ and $\langle n^2 \rangle = 180.58$, and for a primary energy 100 eV, $\langle n \rangle = 27.12$ and $\langle n^2 \rangle = 738.32$. If these histograms had been obtained experimentally with monoenergetic primary particles, the ordinate would be labeled with $N(n)$, the number of primaries yielding n pairs. For example, if 500 primaries were used, the vertical scale would be multiplied by 500. If the envelope of these histograms were Gaussian, as pointed out in Ref. 1, the full width at half maximum of these curves would be $(8FE\ln2/\epsilon)^{1/2}$, or for $\epsilon=3.64$ eV and $F=0.113$, they are 2.93 and 4.15 at $E=50$ and 100 eV, respectively; the values from these histograms are 3 and 4.

functions $p_n(E)$ for selected values of E in Si with $A=5.2$ eV^3 are shown in Fig. 3.

It is seen in Fig. 2 that $\epsilon(E)$ does approach a constant value ϵ at large E, but it does so only for E large compared to $10E_g$. This result could not be shown in Ref. 1 and ϵ had to be approximated by the operational definition $\epsilon=\epsilon_{\bar{k}}(6E_g)$. The function $\epsilon_{\bar{k}}(E)$ from Ref. 1 is shown in Fig. 2. The values of ϵ calculated with the Monte Carlo method, taking $\epsilon=\epsilon(E)$ for E greater than $1000E_g$, differed from those calculated in Ref. 1 by less than 1%, verifying the operational definition.

Likewise, the Fano factor $F(E)$ does approach a constant value F at large E, but only for E large compared to $10E_g$. In Ref. 1, F had to be approximated by $F=F_{\bar{k}}(6E_g)$. The values of F calculated with the Monte Carlo method, taking $F=F(E)$ for E between $50E_g$ and $200E_g$, were near those calculated in Ref. 1.

If the functions $p_n(E)$ approach Gaussians for large E, the skew and kurtosis should approach 0, since the skew and kurtosis are related to the third and fourth moments of $p_n(E)$. The values of these quantities depend strongly on the wings of the functions $p_n(E)$, and they can be reliably calculated only when the number of cascades is very large. For Si with $A=5.2$ eV^3 and E between 20 and $100E_g$, the values of the skew were always less than 0.1, and the absolute values of the kurtosis were always less than 0.2.

III. ELECTROSTATIC ELECTRON-PHONON INTERACTION

A. Scattering rates

The scattering rates for the electron-phonon interaction due to the deformation potential and to the polar-mode electrostatic potential are[5]

$$r'_{\rm DP}(E)=\frac{(KD_t)^2 m^{3/2}(E/2)^{1/2}}{\pi\hbar^3\omega_0\rho} \tag{11}$$

and

$$r'_{\rm PE}(E)=\frac{\hbar\omega_0 \ln(4E/\hbar\omega_0)}{\kappa^* a_0(2mE)^{1/2}}\ , \tag{12}$$

where KD_t is the optical-mode deformation-potential constant (where K has the dimension of reciprocal length and D_t has the dimension of energy), ρ is the semiconductor density, κ^* is the effective dielectric constant,

$$\kappa^{*-1}=\kappa_\infty^{-1}-\kappa_0^{-1}\ ,$$

and a_0 is the Bohr radius. The approximations $kT=0$ and $E\gg\hbar\omega_0$ have been used in Eqs. (11) and (12). The deformation-potential scattering rate has the same energy dependence as was assumed in Ref. 1, namely, $\sqrt{E}$, while the polar-mode electrostatic scattering rate has the energy dependence $E^{-1/2}\ln(4E/\hbar\omega_0)$. Both these scattering modes were incorporated into the Monte Carlo calculation.

In Eq. (20) of Ref. 1, the ratio of $r'_{\rm DP}(E)$ to $r(E)$, the scattering rate due to ionization, was represented as

$$r'_{\rm DP}(E)/r(E)=105A\sqrt{E}/[2\pi(E-E_g)^{7/2}]\ , \tag{13}$$

where, now with $r(E)$ from Eq. (18) of Ref. 1,

$$A=\frac{(KD_t)^2 m^{3/2} 4\pi^5(\hbar^2/2m)^{9/2}}{\pi\hbar^2\sqrt{2}\rho\omega_0\,|M|^2V^2\Delta} \tag{14}$$

from Eq. (11) with M, V, and Δ defined as in Ref. 1. In Ref. 1, A was assigned the value 5.2 eV^3 from the pair-creation energy for Si. Since $r'_{\rm PE}(E)=0$ in Si, an elemental semiconductor, A retains the value assigned in Ref. 1.

The ratio $r'_{\rm PE}(E)$ to $r(E)$ can be similarly represented as

$$\frac{r'_{\rm PE}(E)}{r(E)}=\frac{105B\ln(4E/\hbar\omega_0)}{2\pi\kappa^*\sqrt{E}(E-E_g)^{7/2}} \tag{15}$$

where

$$B=\frac{\hbar^2\omega_0}{a_0\sqrt{2m}}\frac{4\pi^5(\hbar^2/2m)^{9/2}}{|M|^2V^2\Delta} \tag{16}$$

from Eq. (12). This parameter will be assigned a value from the measured pair-creation energy for CdS.

B. Calculations

From Eqs. (14) and (16) for A and B it can be seen that A varies inversely with $\hbar\omega_0$ while B varies directly with $\hbar\omega_0$. Since $\hbar\omega_0$ is a parameter of the theory, it is consistent to extract this dependence from A and B. Thus new constants A' and B' are defined, where $A'=\hbar\omega_0 A$ and $B'=B/\hbar\omega_0$. From $A=5.2$ eV^3 for Si where $\hbar\omega_0=0.063$ eV, $A'=0.328$ eV^4. Following the approach in Ref. 1, the constants A' and B' are assumed independent of the particle energy and invariant for holes and electrons, for different materials, and for all ambient conditions.

The value for B' was determined from the measured value of ϵ for CdS. With the use of A' given above to specify the phonon scattering due to the deformation-potential interaction in CdS, the additional phonon scattering needed to make the calculated value of ϵ equal to the measured value of ϵ in

TABLE I. Calculated and measured values of ϵ.

Semiconductor	E_g [a] (eV)	$\hbar\omega_0$ [a] (eV)	κ^{*-1} [b]	ϵ (eV)	ϵ (expt.)[a] (eV)
Ge	0.735	0.037	0	2.99	2.96
Si	1.12	0.063	0	3.64	3.63
GaAs	1.42	0.034	0.0140	4.31	4.35
CdTe	1.52	0.021	0.0409	4.49	4.46
HgI_2	2.13	0.007	0.143	5.42	4.2
GaP	2.22	0.045	0.0202	5.75	6.54
CdS	2.41	0.038	0.0685	6.30	6.3
AgBr	2.68	0.016	0.133	6.49	5.8
PbO	2.76	0.054	(0.0555)[c]	7.02	8
SiC	2.86	0.120	0.0504	7.86	6.9
AgCl	3.25	0.024	0.162	7.65	7.5
C	5.47	0.163	0	10.8	13.1
SiO_2	8.9	0.081	0.241	18.0	18

[a] Reference 1.
[b] Reference 6.
[c] Estimated.

CdS was used to determine B'. This value is $B'=4000$ eV^3. These values of A' and B' were used to calculate the values of ϵ which are shown in Table I. These calculations were done for initial energies between $4000E_g$ and $5000E_g$ and up to 50 cascades. The uncertainties in ϵ were always less than 0.03 eV, and frequently less than 0.01 eV. The measured values of ϵ are also shown in Table I. The values of κ^{*-1} were obtained from the sources listed in Ref. 6. The measured and calculated values of ϵ are plotted in Fig. 4. This choice of B' is seen to give excellent agreement between the measured and calculated values of ϵ for GaAs and CdTe as well as CdS; the measurements for these three semiconductors are among those done most recently.

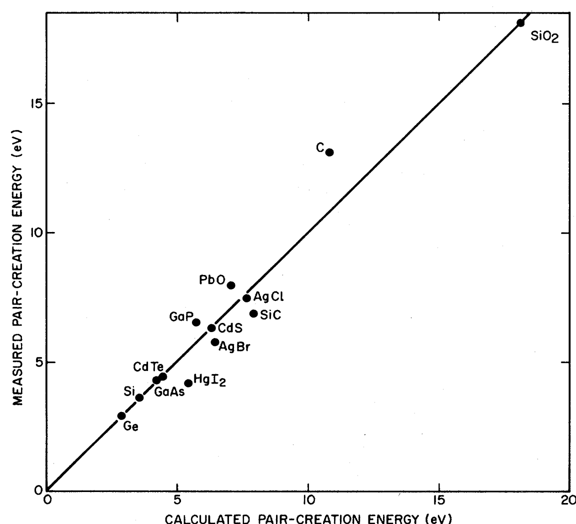

FIG. 4. Measured values of the pair-creation energy, listed in Table I, are plotted vs the calculated values of ϵ, also listed in Table I. The straight line has unit slope and is the lower bound expected for the measured values.

The additional electron-phonon scattering mechanism in the binary semiconductors must increase the values calculated for ϵ, and these values are lower bounds on ϵ. Since the measured and calculated values of ϵ in Ref. 1 were nearly equal for some semiconductors, now the measured values of ϵ are smaller than the calculated values for some semiconductors. It must be concluded, therefore, that either the measurements or the theory is in error; the limitations on the theory are discussed in Sec. IV. Nevertheless, the increases in the calculated values of ϵ are generally small, the largest being 18%. In fact, the general agreement between the calculated and measured values shown in Fig. 4 is as good as that shown in Fig. 8 of Ref. 1.

No additional electron-phonon scattering mechanism was added for the elemental semiconductors, and no changes were made in the parameter A for Si. For Ge, the use of A' instead of A increased the value calculated for ϵ; this improved the agreement of the calculated and measured values. For diamond, the use of A' instead of A decreased the value calculated for ϵ; the measured value is still much larger than the calculated value.

Calculations of the Fano factor were done for 5000 cascades with initial energies of about $100E_g$. The calculated Fano factors were 0.113 ± 0.005 for Si and 0.126 ± 0.005 for Ge. These values are near those reported in Ref. 1 and in good agreement with the measured values.

IV. DISCUSSION

A. Crazy Carpentry

Van Roosbroeck[2] also used the Monte Carlo method to calculate ϵ and F in 1965. He introduced the method to verify an analysis called "crazy carpentry." The basic assumptions used in Refs. 1 and 2 are equivalent.[3] The differences arise from the particular assumptions made to perform the calculations. For example, (1) in crazy carpentry the ratio of the scattering rates shown in Eq. (13) above was assumed constant for all energies, while in Ref. 1, the ratio of scattering matrix elements, A of Eq. (14), is assumed constant. No distinction was made between the various electron-phonon interactions in either Refs. 1 or 2. Also, (2) the newly created particles in Ref. 2 were assumed to have equal energies, i.e., $dq_2/d\alpha_2$ was set to $\delta(\alpha_2-0.5)$ in Fig. 1. Finally, (3) the density of states was assumed constant in the formulation of Ref. 2.

For $A=0$, the first difference mentioned above is nullified. The function $dq_2/d\alpha_2$ was changed to $\delta(\alpha_2-0.5)$ to evaluate the effects of the second difference. The calculated value of ϵ was not affected significantly, and, indeed, as noted in Ref. 1, both calculations gave similar values for ϵ when $A=0$. The calculated value of F was significantly affected, however. The value was consistent with the value 0.125 61 given in Ref. 2, but the value calculated with the $dq_2/d\alpha_2$ shown in Fig. 1 was consistent with the value 0.08 given in Ref. 1. When the density of states function was changed to evaluate the effects of the third difference, little change in the calculated values of ϵ and F was found.

B. Optical-phonon deformation-potential constant

As is described in greater detail in Ref. 7, the constants A' and B' contain two unknown quantities, the matrix element of the Coulomb interaction and KD_t, the deformation-potential constant. From the values assigned empirically to A' and B', the value

$$KD_t=2\sqrt{\rho}\times10^8 \tag{17}$$

in units of eV/cm, where ρ is the numerical value of the semiconductor density in g/cm^3, was obtained. As discussed in Ref. 7, this value is consistent with the values reported from transport measurements in Ge and Si. In Raman scattering measurements, a deformation-potential constant $d=2aKD_t$, where a is the lattice constant, is measured.[8] Again the value given in Eq. (17) is consistent with the values of d from Raman scattering measurements and with values calculated from pseudopotential theory.[8]

This value of KD_t may be used in Eq. (11) to estimate the absolute value of the phonon scattering rate, i.e., $r'_{\rm DP}(E)=5\times10^{11}(\sqrt{E}/\hbar\omega_0)\ \sqrt{\rm eV}$/sec. The rate obtained for 1.5-eV electrons in GaAs, $2\times10^{13}\ {\rm sec}^{-1}$, is in good agreement with the rate estimated from the electric field strength required for impact ionization.[9]

C. Rare-gas solids

Recently measurements of ϵ in several rare-gas solids have been reported.[10] These materials, Xe, Kr, and Ar, have larger band gaps,[11] 9.3, 11.6, and 14.2 eV, respectively, than any of the materials shown in Table I. These band gaps are so large, in fact, that phonon scattering should not contribute significantly to ϵ, i.e., the calculated lower bounds on ϵ should be only slightly larger than the values calculated for $A=0$. For the ionization threshold energies given in Eqs. (22) and (23) of Ref. 1, these values are $2.04E_g$ and $1.62E_g$. Thus unlike the semiconductors discussed in Ref. 1, the calculated values of ϵ for these materials are sensitive to differences in the threshold energies for ionization. The measured value of ϵ for Xe, 24 eV, is well above the calculated lower bounds using either of these thresholds. The measured values for Kr and Ar, 25 and 27 eV, respectively, cast doubt on the validity of using the threshold energies given by Eq. (22) of Ref. 1, i.e., those obtained from the free-particle model with momentum conservation. All the measured values are consistent with Eq. (23), which was obtained without momentum conservation and used in the calculations of Secs. II and III above.

D. Mercuric iodide

From Fig. 4 it is apparent that three semiconductors, HgI_2, AgBr, and SiC, have measured values of ϵ well below the calculated lower bounds. Two of these, HgI_2 and AgBr, have the smallest values of $\hbar\omega_0$ of any of the semiconductors listed in Table I. To see how small values of $\hbar\omega_0$ might change the calculations, the effect of finite temperature was included in the Monte Carlo calculations. Also, the dependence of ϵ on $\hbar\omega_0$ was examined to see how electron-phonon scattering vanishes for small $\hbar\omega_0$.

At finite temperatures, i.e., when $kT\geq\hbar\omega_0$, there is scattering with phonon absorption as well as with phonon emission. The absorption rate is proportional to

$$n_0=[\exp(\hbar\omega_0/kT)-1]^{-1}\,,$$

and the emission rate is proportional to n_0+1. The temperature dependences of $\epsilon(E)$ and $F(E)$ were modeled by setting the phonon scattering rate pro-

portional to $2n_0+1$ and including phonon absorption with probability $n_0/(2n_0+1)$. For the parameters of HgI_2 no temperature dependence could be found for either $\epsilon(1000\text{ eV})$ or $F(100\text{ eV})$. The increased phonon scattering was balanced by the decreased net phonon emission.

The relationship of ϵ to $\hbar\omega_0$ was calculated for the parameters of HgI_2 and initial energies of 1000 eV. The value of ϵ grew with increasing $\hbar\omega_0$, as expected, and in the limit as $\hbar\omega_0$ approached zero, ϵ approached 5.4 eV. However, the removal of electron-phonon scattering, i.e., setting $A'=B'=0$, gives $\epsilon=3.5$ eV. Physically, this difference in these two values of ϵ is unacceptable, as they both represent the absence of phonon scattering. The difference arises because of the inverse dependence of $r'_{\rm DP}(E)$ on $\hbar\omega_0$ in Eq. (11), and this dependence comes from the specification of the vibrational amplitude in the deformation-potential theory.[12] Thus the assumption that A' is the same for all materials does not extend to materials with very low $\hbar\omega_0$.

The value of $F(100\text{ eV})$ calculated for the parameters of HgI_2 was 0.10 ± 0.01. The value calculated for $A'=B'=0$ was 0.08 ± 0.01. Both these values are far below the present experimental[13] upper bound on F, 0.19 ± 0.03.

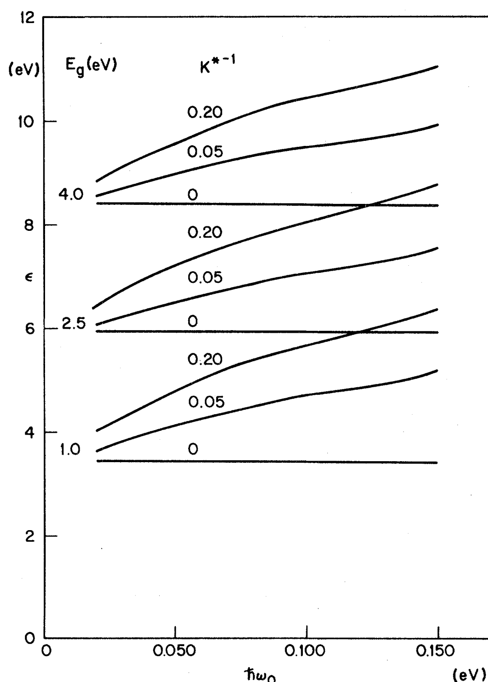

FIG. 5. Calculated values of ϵ are plotted vs $\hbar\omega_0$ for values of E_g of 1.0, 2.5, and 4.0 eV and values of κ^{*-1} of 0, 0.05, and 0.20. Each calculation of ϵ was done for ten cascades having initial energies of $4000E_g$. The uncertainties in ϵ were 0.10 eV or less.

E. Large phonon energies

In Ref. 1 ϵ was calculated as a function of E_g and $\hbar\omega_0$ with a single value of A. In this paper ϵ has been calculated as a function of E_g, $\hbar\omega_0$, and κ^{*-1} with single values of A' and B'. The dependence of ϵ on $\hbar\omega_0$ is shown in Fig. 5 for selected values of E_g and κ^{*-1}. It is apparent in Fig. 5 that for $\kappa^{*-1}=0$, i.e., for scattering due to the deformation potential alone, ϵ is virtually independent of $\hbar\omega_0$. This result is consistent with the observation made in Ref. 3 that the term in the energy-loss rate due to the deformation potential is insensitive to ω_0. In the context of Eq. (14), doubling ω_0 halves A but doubles the energy loss per phonon scattering event, so the net loss is unchanged.

For nonzero values of κ^{*-1}, the values of ϵ shown in Fig. 5 grow with increasing ω_0. This growth, as observed in Ref. 3, is due to the direct dependence of B on ω_0 in Eq. (16). The contribution to ϵ due to the polar-mode electrostatic potential dominates the contribution due to the deformation potential when $\frac{1}{2}[\epsilon(\kappa^{*-1})-E_g]$ exeeds $[\epsilon(\kappa^{*-1}=0)-E_g]$. Thus, with the use of Fig. 5, for $E_g=1.0$ eV and $\kappa^{*-1}=0.20$, the polar-mode electrostatic potential makes the larger contribution to ϵ for $\hbar\omega_0\gtrsim0.125$ eV. For this value of κ^{*-1} and larger values of E_g, larger values of $\hbar\omega_0$ are required for the polar-mode electrostatic potential to make the larger contribution to ϵ. As seen from Table I here and from Table I of Ref. 14, materials with $\kappa^{*-1}\gtrsim0.20$ and $\hbar\omega_0\gtrsim0.125$ eV are uncommon. Thus materials may occur for which the polar-mode electrostatic contribution is the dominant contribution from the electron-phonon interaction, but they do not occur frequently.

F. Cathodoluminescent efficiency

As was pointed out in Ref. 1, the upper bound on the cathodoluminescent efficiency of a cathode-ray phosphor is $\xi=E_e/\epsilon$, where E_e is the energy of the photon emitted by the phosphor, i.e., an electron-hole pair yields at most one photon. Values of ξ were calculated for a number of well-known phosphors using the values of E_g, $\hbar\omega_0$, κ_0, and κ_∞ given in Table I of Ref. 14 to calculate ϵ, and the values of E_e given in Table II of Ref. 14 to calculate ξ. The measured efficiencies, from Ref. 14, are plotted versus ξ in Fig. 6. It can be seen in Fig. 6 that in no case does the measured efficiency exceed ξ.

In Ref. 14 the "crazy carpentry" analysis of Ref. 2 was extended to explicitly include the phonon scattering due to the polar-mode electrostatic interaction; scattering due to the deformation potential was ignored. Since the parameter B, which described scattering due to the polar-mode electro-

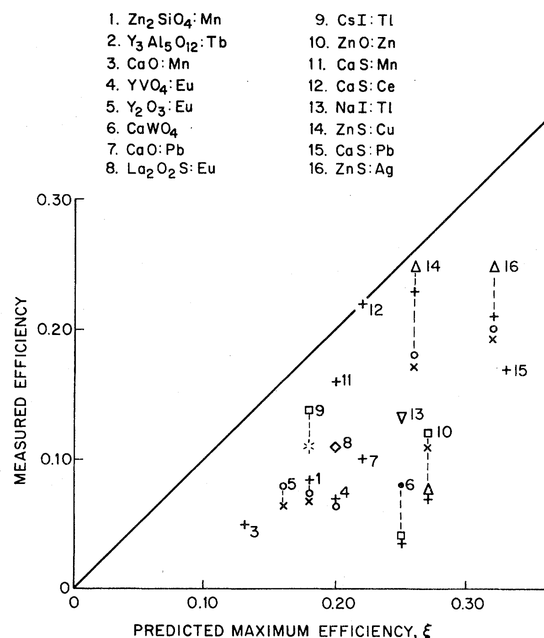

FIG. 6. Measured values of the cathodoluminescent efficiency are plotted vs the predicted upper bound ξ on the efficiency. This figure is identical to Fig. 5 of Ref. 14 except for the new calculations of ξ described here. The straight line has unit slope and is the upper bound expected for the measured values. The code for the measured values is the same as in Ref. 14. The calculations of ϵ were done for initial energies between 4000 and $5000E_g$ and up to 50 cascades.

static interaction, depends on $\hbar\omega_0$, a strong dependence of ξ on $\hbar\omega_0$ and κ^{*-1} was found in Ref. 14, and the values of ξ spanned a broad range. Here, however, both interactions have been considered, and scattering due to the deformation potential is always present. The deformation-potential constant is insensitive to the parameters of the semiconductor, so the values of ξ span a narrower relative range in Fig. 6 than in Fig. 5 of Ref. 14.

The largest measured efficiencies are seen in Fig. 6 to occur in ZnS and CaS. The values of ξ for these materials span more than half the total range of ξ in Fig. 6. Thus the singular property of these materials responsible for the large efficiencies does not seem to be associated with ξ. In summary, the measured phosphor efficiencies are consistent with calculations of the pair-creation process, but the material property that makes ZnS and CaS so highly efficient is not associated with this process.

V. SUMMARY

The probability method, based on the scattering-rate assumption, for calculating the pair-creation energy, was described in Ref. 1. In Ref. 1 the energies were calculated with a recursion method. In this paper these same energies were calculated with the Monte Carlo method. The identity of the values obtained for the pair-creation energies from these two calculations corroborates the values. Since either method of calculation, the recursive or Monte Carlo, can be used with the "probability method," it should perhaps have been called the "probability procedure."

In Ref. 1 values of $\epsilon(E)$ could only be calculated for energies E up to about $10E_g$. These energies were far too low to allow a direct estimate of the asymptotic value of $\epsilon(E)$ for large E, and an indirect estimate had to be made. With the Monte Carlo method, values of $\epsilon(E)$ can be calculated for energies beyond $100\,000E_g$ and a direct estimate of the asymptotic value can be made. The agreement of the indirect estimates from Ref. 1 and the direct estimates obtained here corroborates the values.

In Ref. 1 only limited account was taken of the scattering by phonon emission. In particular, the square of the matrix element was proportional to a constant, labeled A, which was assumed independent of the particle energy and invariant for different materials. In fact, there are at least two distinct electron interactions which result in phonon emission. In the free-electron approximation, these two interactions, the deformation-potential and the polar-mode electrostatic interaction, have matrix elements which depend differently on the particle energy. While that of the deformation potential is independent of particle energy, that of the polar-mode electrostatic interaction does depend on energy. Furthermore, both these matrix elements contain the optical-phonon energy, which is different for different materials.

In this paper both these electron-phonon interactions were considered. The factors of the matrix elements containing the particle energy and the optical-phonon energy were explicitly retained in the calculation. Aside from fundamental constants, the only remaining factors in these matrix elements are the material density and the deformation-potential constant in the deformation-potential interaction and the effective dielectric constant in the polar-mode electrostatic interaction. The effective dielectric constants were taken from experimentally measured data. Since the assumptions of independence of particle energy and invariance for all materials were separately made for A' and B', the ratio of the deformation-potential constant and square root of the material density has a constant value.

This treatment of the electron-phonon interaction changed the values calculated for $\epsilon(E)$ and $F(E)$ from the values given in Ref. 1 for all materials ex-

cept Si. The changes were generally small, indicating the insensitivity of ϵ to the added polar-mode electrostatic scattering. Because the changes are small, the conclusions reached in Ref. 1 remain generally valid.

ACKNOWLEDGMENTS

The author is indebted to S. Bloom, C. Struck, and M. Inoue for their many helpful comments.

[1]R. C. Alig, S. Bloom, and C. W. Struck, Phys. Rev. B 22, 5565 (1980). (This is paper I.)

[2]W. van Roosbroeck, Phys. Rev. 139, A1702 (1965).

[3]M. Inoue, Phys. Rev. B 25, 3856 (1982).

[4]International Mathematical and Statistical Libraries, Inc. Routine GGUBFS, IMSL Library, 7500 Bellaire Blvd., Houston Texas 77036.

[5]E. M. Conwell, *High Field Transport in Semiconductors* (Academic, New York, 1967).

[6]The values of κ_0 and κ_∞ were taken from E. Kartheuser, in *Polarons in Ionic Crystals and Polar Semiconductors,* edited by J. T. Devreese (North-Holland, Amsterdam, 1972), p. 717; from R. Minder, G. Ottoviani, and C. Canali, J. Phys. Chem. Solids 37, 417 (1976), for HgI_2; and from C. Denau, J. Phys. Radium 24, 284 (1963), for SiO_2.

[7]R. C. Alig, S. Bloom, and M. Inoue, J. Phys. (Paris) 42, C6-484 (1981).

[8]W. Potz and P. Vogl, Phys. Rev. B 24, 2025 (1981).

[9]F. Capasso, T. P. Pearsall, K. K. Thornber, R. E. Nahory, M. A. Pollack, G. B. Bachelet, and J. R. Chelikowsky, J. Appl. Phys. 53, 3324 (1982).

[10]W. E. Spear and P. G. LeComber, in *Rare Gas Solids,* edited by M. L. Klein and J. A. Venables (Academic, London, 1977), p. 1119.

[11]V. Rössler, in *Rare Gas Solids,* Ref. 10, p. 505.

[12]W. A. Harrison, Phys. Rev. 104, 1281 (1956).

[13]G. R. Ricker, J. V. Vallerga, A. J. Dabrowski, J. S. Iwanczyk, and G. Entine, Rev. Sci. Instrum. 53, 700 (1982).

[14]D. J. Robbins, J. Electrochem. Soc. 127, 2694 (1980).